Longitudinal coherence and short-term wind speed prediction based on a nacelle-mounted Doppler lidar

M. Debnath[1], P. Brugger[2], E. Simley[1], P. Doubrawa[1], N. Hamilton[1], A. Scholbrock[1], D. Jager[1], M. Murphy[1], J. Roadman[1], J. K. Lundquist[1,3], P. Fleming[1], F. Porté-Agel[2], P. Moriarty[1]

[1] National Renewable Energy Laboratory, Colorado, USA
[2] École polytechnique fédérale de Lausanne, Lausanne, Switzerland
[3] University of Colorado, Boulder, Colorado, USA

E-mail: mithu.debnath@nrel.gov

Abstract. The spatial structure of turbulence in atmospheric boundary layer flows is highly relevant to wind energy. In particular, wind turbine control strategies based on inflow preview measurements require knowledge of the longitudinal evolution of turbulent flow as it approaches the rotor. These upstream measurements are usually obtained with nacelle-mounted wind lidars. In contrast to traditional *in situ* anemometry, lidars collect measurements within a probe volume which varies in size depending on the technology of the commercial system being used. Here, we address two issues related to the use of wind lidar to measure the incoming flow to a wind turbine: (i) whether existing longitudinal coherence models can be used to predict flow at the rotor, based on measurements performed at a distance away from the rotor; and (ii) what effect probe-volume averaging has on the inflow predictions. These two questions are critical to the design and implementation of robust wind turbine control strategies. To address these questions, we perform field measurements and large-eddy simulations to determine which incoming flow structures can be readily predicted with existing coherence models, and which require additional corrections to account for lidar volumetric averaging effects. Results reveal that the wind turbine induction zone has a negligible impact on the longitudinal coherence and first-order turbulence quantities, such as the standard deviation of velocity fluctuations. However, the phase of the signal, from which advection time periods of the turbulent structures are derived, is affected by the rotor blockage effect.

1. Introduction

Substantial gains in wind power plant performance and reliability can be achieved if wind turbines have preview information about the flow that is approaching to them and can predict its evolution in time to make flow-informed control decisions [1, 2]. This inflow preview capability can be achieved with forward-facing, nacelle-mounted lidars, which provide volume-averaged line-of-sight velocity measurements upstream of a wind turbine. However, no models currently exist that can accurately estimate the spatial and temporal evolution of the measured flow structures as they advect toward the turbine and also respond to its thrust.

Inflow preview measurements are often taken far upstream (i.e., 300 m) so that the turbine has enough time to respond appropriately. The advection time of the measured flow is often estimated based on the frozen turbulence hypothesis [3], which is not valid for all turbulent eddy scales described by coherence models [4]. The downstream evolution of the measured

turbulence structures predicted by this hypothesis and existing coherence models [5, 6] has not been extensively validated. Lidar is a powerful tool for measuring the wind speed of atmospheric structures along the mean wind direction and can be used to validate coherence models. However, probe-volume averaging poses a limitation on the length-scales and time-scales that the lidar can resolve, and needs to be considered when developing and validating coherence models based on lidar data.

In addition, for inflow preview to be successfully realized, the frozen turbulence hypothesis and coherence models need to be evaluated in detail and improved to include the effects of rotor induction [7, 8]. Here, we use high-resolution field measurements and high-fidelity numerical simulations to investigate the evolution of turbulence structures as they advect toward a utility-scale operational wind turbine, both in the freestream and within the induction zone. We quantify the effect of the induction zone on the incoming flow and investigate whether existing longitudinal coherence models can accurately predict the evolution of turbulence structures along the mean wind direction.

The results presented herein compare the performance of existing longitudinal coherence models, both in freestream and the induction zone, and discuss the limitations of lidar for measuring the coherence of atmospheric turbulence. These insights will be useful for future validation studies, coherence model improvements, and analysis of field measurements collected for wind turbine control based on inflow preview.

2. Scanning lidar measurements

A Halo Photonics scanning lidar was placed on top of the nacelle of a GE 1.5-MW turbine with hub height, $H = 80$ m and diameter, $D = 77$ m. The range-gate spacing of the lidar is 18 m, and the lidar stared upstream of the turbine with an azimuth and elevation angle equals zero. The data collection frequency was 0.83 Hz, which provides an opportunity for analyzing turbulent eddies of a higher equivalent wavenumber. The lidar scanned intermittently for approximately 1 week for the purpose of this study, and the data have been quality controlled based on the signal-to-noise ratio and turbine operational status. After the quality control, only three different cases were found that have separate atmospheric properties. Descriptions of the cases are provided in Table 1. Case01 is close to a laminar flow with turbulence intensity, $TI = 1.24\%$ with z/L_i of 0.42, where L_i is the Obukhov length. The Obukhov length, L_i, is calculated based on Eq. 1, and measurements needed for the calculation come from a meteorological tower. The met tower has a sonic anemometer at height 10 m along with pressure, humidity, and temperature sensors at heights of 5 m, 2 m, and 2 m, respectively.

$$L_i = -\frac{u_\star^3 T_v}{kg\overline{w'T_s'}} \tag{1}$$

where, $u_\star$ is friction velocity, k is the von Kármán constant, T_v is virtual temperature, and $\overline{w'T_s'}$ is the heat flux.

The integral length-scale, L is defined as:

$$\begin{aligned} L &= U * T_{xx} \\ T_{xx} &= \int_0^\infty u(t)u(t+\tau)d\tau \end{aligned} \tag{2}$$

where T_{xx} is the integral time-scale, U is the mean wind speed of the signal, and u is the fluctuating component of the signal. T_{xx} is estimated with the area under the autocorrelation of the signal which is a function of lagged time, and a threshold of 0.05 is considered instead of zero-crossing [5] to calculate the area under the autocorrelation function. The length-scales provided in Table 1 for the respective cases might not be a good representation of the cases.

The lidar data have low sampling frequency and larger probe volume which can create bias in the length-scale estimation. This issue will be discussed later in section 4.

Data measured during a 10-minute period by the Doppler lidar are shown for Case01 and Case03 in Figure 1. The measurements qualitatively show the advection and evolution of the wind field toward the wind turbine (Figure 1, top row) and the induction zone when a temporal average is applied (Figure 1, middle row). The evolution of the wind field over the distance can be seen as a decrease of coherence for increasing separation distances (Figure 1, bottom row). The magnitude of wind coherence is calculated as: cross-power spectral density (CPSD) between the signals divided by the power spectral density (PSD) of individual signal (shown later, Eq. 7). The drop of the coherence with increasing separation distance calls into question the advection time and length-scales that can be predicted with the lidar data. Phase angles are calculated by taking the real and imaginary parts of the CPSD between the signals. The frequency at which the phase angle peaks before returning to zero is used to calculate the maximum size of the turbulent eddies advected by the mean wind speed (Figure 2a,b). The maximum coherent wavenumbers corresponding to the phase angle peaks are plotted in Figure 2c. Turbulent structures that advect along the mean wind direction decay exponentially with separation distances. An example of the prediction of wind speed signals based on the predicted maximum coherent wavenumber is provided in Figure 3. The downstream signal is shifted in time based on the upstream wind speed and filtered based on the predicted wavenumber, providing a clear visualization of the advected structures.

Table 1: Description of the cases used in this study

Cases	Mean Wind Speed, U_h (m/s)	Turbulence Intensity, TI (%)	Length-scale, L (m)
Case01	9.74	1.24	477
Case02	14.89	11.3	603
Case03	11.59	3.51	142

3. Computational fluid dynamics simulation and virtual lidar

The Simulator fOr Wind Farm Applications (SOWFA) [9], a large-eddy simulation tool developed by the National Renewable Energy Laboratory, is used in this study to simulate a neutral atmospheric boundary layer with a mean wind speed of 8 m/s and hub height turbulence intensity of 8.35%. An actuator line model is used to model the wind turbine. The virtual lidar measures at points along the line-of-sight (LOS) and provides LOS wind speed measurements according to:

$$v_{\mathrm{los}}(r) = U_h(r)\cos\phi\cos(\theta-\theta_0) + w(r)\sin\phi \tag{3}$$

where U_h is the horizontal wind speed, r represents the range along the laser beam, ϕ is the elevation angle, θ is the azimuth angle, and θ_0 is the wind direction; and v_{los} is the LOS velocity obtained at the corresponding point. With $\phi = 0$ and $\theta = \theta_0$, $v_{\mathrm{los}}(r) = U_h$.

A weighting function is applied to the point measurements to take into account the volume-averaging imposed by the lidar. The weighting function is applied along the length of the laser beam, assuming the beam is very narrow in the transverse direction [10, 11]:

$$v_{\mathrm{los,eq}}(F) = \int_0^\infty v_{\mathrm{los}}(r)W(F,r)\mathrm{d}r \tag{4}$$

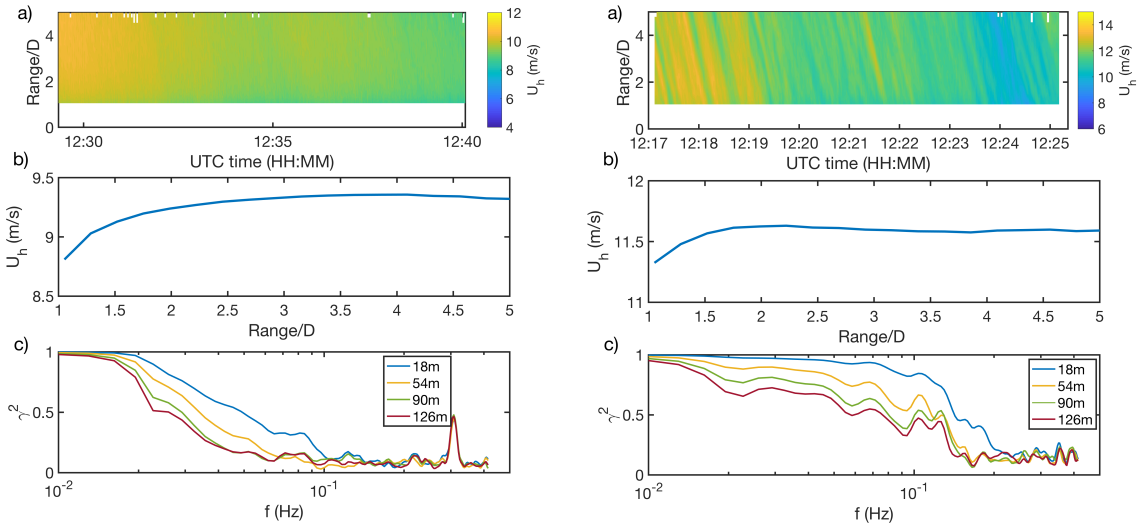

(a) Case01 data set (b) Case03 data set

Figure 1: Lidar data sets and quantitative visualization. a) Horizontal wind speed data collected with lidar, U_h (m/s); b) 10-min averaged wind speed; and c) coherence with different separation distances.

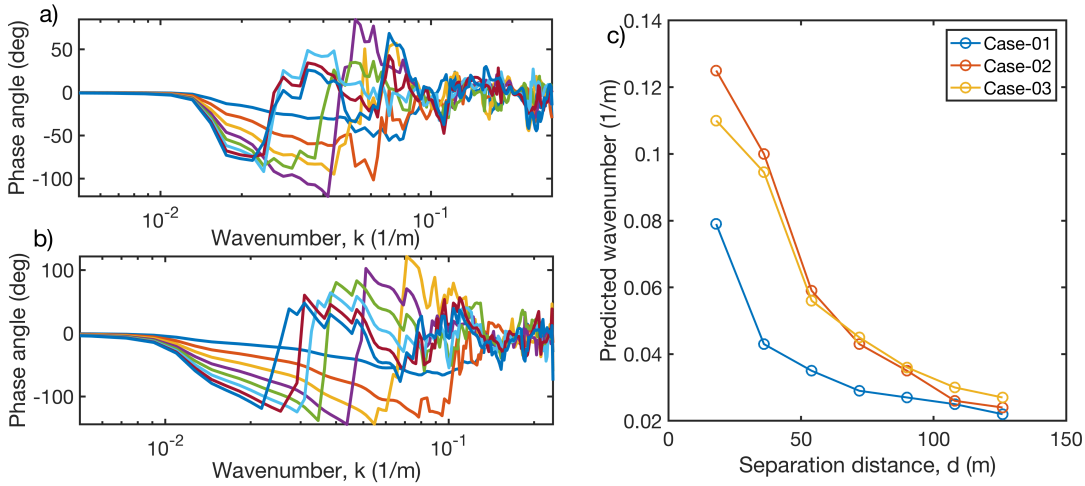

Figure 2: Wind speed phase information for different longitudinal separation distances. a) Phase angle with separation distances, $d = 18$ m to $d = 126$ m with an increment of 18 m for Case01; b) phase angle with different separation distances (same as Case01) for Case03; and c) maximum coherent wavenumber for turbulent structures.

where F is the distance along the beam from the lidar to the intended measurement point, and $W(F, r)$ is the weighting function. The weighting function for pulsed lidars derived by Frehlich *et al.* [12] is used here:

$$W(F,r) = \frac{1}{2\Delta_\mathrm{p}} \left(\mathrm{Erf}\left(\frac{r - F + \frac{\Delta_\mathrm{p}}{2}}{\frac{\Delta_\mathrm{r}}{2\sqrt{\ln 2}}} \right) - \mathrm{Erf}\left(\frac{r - F - \frac{\Delta_\mathrm{p}}{2}}{\frac{\Delta_\mathrm{r}}{2\sqrt{\ln 2}}} \right) \right), \tag{5}$$

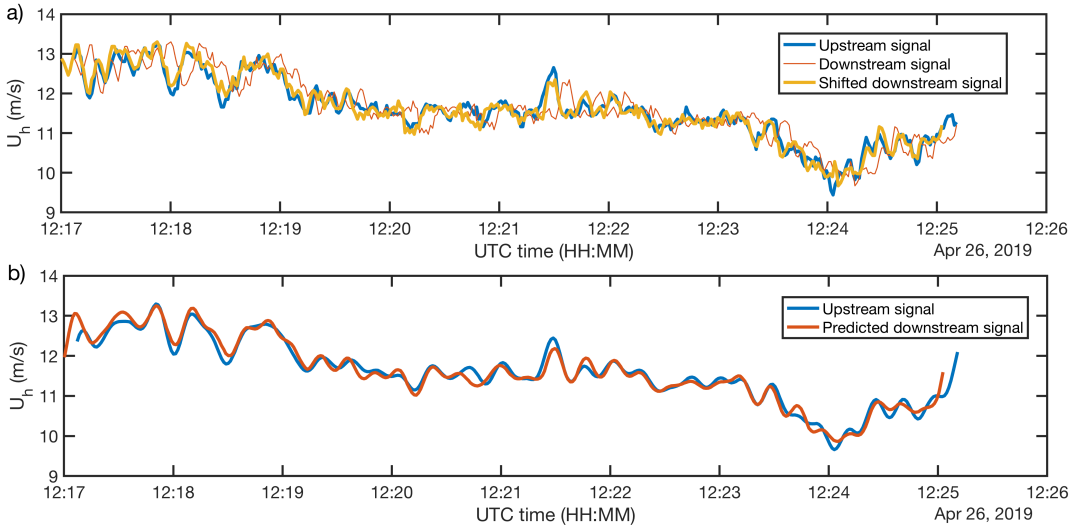

Figure 3: Prediction of turbulent structures that advect at the mean wind speed. a) Two signals longitudinally separated by 90 m; b) shifted wind speed signal filtered based on the maximum coherent wavenumber for 90 m separation distance from Figure 2c.

where Δ_p is the range-gate spacing and Δ_r is the full-width-at-half-maximum pulse width. To approximate the Halo Photonics lidar system, we use values of $\Delta_\mathrm{p} = 18$ m and $\Delta_\mathrm{r} = 24.5$ m.

4. Treatment of the lidar-measured coherence

Wind coherence or spatial variability of wind are dictated by atmospheric conditions, in particular, atmospheric stability. The coherence plot (Figure 1c) and cases chosen in this study (Table 1) confirm that the coherence model should consider the atmospheric conditions. The theoretical equation for longitudinal coherence used here is chosen based on previous work by [13, 14]. The exponential decay coherence function contains parameters that can be tuned to represent different atmospheric conditions:

$$\gamma(f,d)^2 = \exp\left(-a\sqrt{(\frac{fd}{U})^2 + (bd)^2}\right), \tag{6}$$

where a and b are tuning parameters that serve to distinguish the dependence on the atmospheric conditions. In previous work on modeling longitudinal coherence [15, 14], the standard deviation, σ, and length-scale, L, were chosen to characterize the properties of the signals. Work presented in [14] derived a and b parameters based on numerical simulations. However, σ and L derived from the lidar signals are not accurate, for reasons that will be discussed further later. High-frequency lidar measurements have previously been used to calculate turbulence characteristics, such as longitudinal coherence [6, 7]. However, because of the restriction to LOS velocity measurements and the lidar probe volume, care must be taken when comparing turbulence quantities measured by a lidar with those representing point measurements of individual velocity components. To determine how well the different theoretical longitudinal coherence models evaluated here match field observations, we compute the theoretical coherence between wind speeds measured at different lidar range gates.

Letting $v_{\mathrm{L}i}$ represent the LOS velocity measured by the lidar at range gate, i, the theoretical

coherence between measurements at range gates, i and k, is defined as

$$\gamma_{v_{\mathrm{L}i}v_{\mathrm{L}k}}(f)^2 = \frac{\left|S_{v_{\mathrm{L}i}v_{\mathrm{L}k}}(f)\right|^2}{S_{v_{\mathrm{L}i}v_{\mathrm{L}i}}(f)S_{v_{\mathrm{L}k}v_{\mathrm{L}k}}(f)}, \tag{7}$$

where $S_{v_{\mathrm{L}i}v_{\mathrm{L}k}}(f)$ is the CPSD between $v_{\mathrm{L}i}$ and $v_{\mathrm{L}k}$, and $S_{v_{\mathrm{L}i}v_{\mathrm{L}i}}(f)$ indicates the power spectral density (PSD) of $v_{\mathrm{L}i}$. To simplify the analysis, we assume that the lidar beam is perfectly aligned with the longitudinal direction.

Using Eq. 4 together with Fourier properties [7, 14], $S_{v_{\mathrm{L}i}v_{\mathrm{L}k}}(f)$ can be calculated as

$$S_{v_{\mathrm{L}i}v_{\mathrm{L}k}}(f) = \int_0^\infty \int_0^\infty W\left(F_i, r_1\right) W\left(F_k, r_2\right) S_{u(r_1)u(r_2)}\left(f\right) \mathrm{d}r_1 \mathrm{d}r_2, \tag{8}$$

where F_i represents the measurement distance of range gate, i, and $S_{u(r_i)u(r_k)}\left(f\right)$ is the CPSD between the longitudinal u velocity components at distances, r_1, and r_2 along the beam. Relying on the definition of magnitude-squared coherence (e.g., Eq. 7) and assuming that the PSD $S_{u(r)u(r)}\left(f\right)$ is independent of the range, r, along the beam, the CPSD between $u\left(r_1\right)$ and $u\left(r_2\right)$ can be expressed as

$$S_{u(r_1)u(r_2)}\left(f\right) = S_{uu}\left(f\right)\sqrt{\gamma^2_{u(r_1)u(r_2)}\left(f\right)}e^{j2\pi(r_2-r_1)f/U}, \tag{9}$$

where $\gamma^2_{u(r_1)u(r_2)}\left(f\right)$ is given by the longitudinal coherence model being evaluated and $2\pi\left(r_2-r_1\right)f/U$ yields the phase delay between velocities separated by distance, r_2-r_1, for mean wind speed, U, based on Taylor's frozen turbulence hypothesis [3]. Note that because of the assumption that $S_{u(r)u(r)}\left(f\right)$ is independent of the range, r, Eq. 7 does not depend on the PSD, $S_{uu}\left(f\right)$. Therefore, a specific turbulence PSD does not have to be assumed when computing the theoretical lidar-measured coherence.

In the freestream region, coherence models by [4, 5] have been considered for comparison of the lidar-measured coherence. Simley et al. [5] derived a model based on large-eddy simulations considering different atmospheric stability conditions; this model is chosen to investigate the impact of lidar volume averaging on the measured coherence, according to Eq. 8 (Figure 4). Once volume averaging is applied to the theoretical model (Simley model) according to Eq. 8, the impact of the volume averaging can be visualized, denoted as "Simley model weighted" in Figure 4. It is clear both from lidar measurements and Simley's model with volume averaging, that lidar overestimates coherence for low wavenumbers and underestimates coherence for high wavenumbers. Volume averaging effectively imparts smoothing to the wind speed signal for low wavenumbers and increases the estimate of coherence, γ^2. On the other hand, volume averaging attenuates the energy of the signal for higher wavenumbers and decreases the coherence. It should be noted that even though the lidar range gate and other optical properties do not vary throughout a field campaign, the impact of the volume averaging varies based on the wind speed signal itself. The general formulation provided in Eq. 8 accounts for variations based on the properties of the wind speed.

The lidar-measured coherence with a separation distance of $d = 36$ m is shown in Figure 4 for the three different cases. The comparison between lidar-measured coherence and theoretical coherence is provided in the first column (Figure 4a, d, g). Simley's model performs well only for Case02, where turbulent structures are larger and volume-averaging effects are limited (Figure 4d). The fitting parameters, a and b, depend on the standard deviation, σ, and length-scale, L, derived from the observed signal. Due to volume averaging, values of σ and L calculated from the lidar signal exhibit some bias.

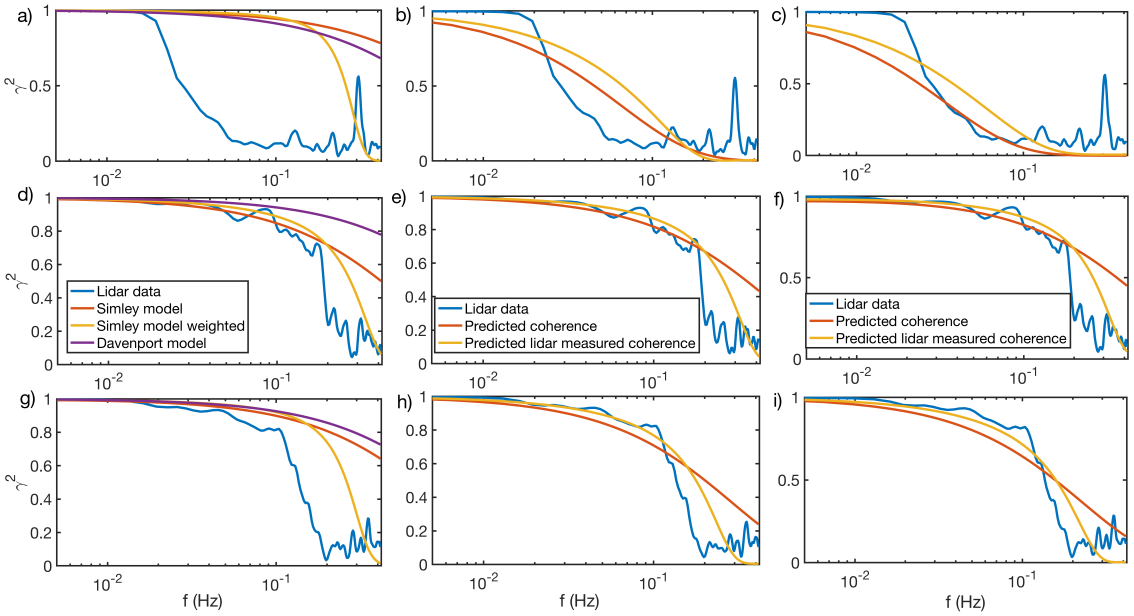

Figure 4: Coherence from lidar measurements and predicted coherence for Case01 (top row), Case02 (middle row), and Case03 (bottom row) with separation distance, $d = 36$ m. a, d, g) Coherence from lidar measurements and theoretical predicted coherence for Case01, Case02, and Case03, respectively; b, e, h) least-squares fitting of the coherence model (Eq. 6) to the lidar-measured coherence; c, f, i) least-squares fitting of the coherence model (Eq. 6), including volume averaging, to the lidar-measured coherence.

Table 2: Fitting parameters from lidar data for different cases

Cases	a, b Simley	a, b least square fitting	a, b minimization problem
Case01	0.16065, 0.000119	4.12737, 2.26e-08	7.896, 3.362e-06
Case02	0.69038, 8.919e-05	0.834305, -9.43e-08	0.82814, 7.65e-06
Case03	0.34338, 0.000535	1.11702, -5.053e-08	1.4356, 9.225e-08

To understand the bias, help from the numerical simulation is considered. Within SOWFA, a virtual lidar is placed at the hub of the turbine, and data are collected in the same way as for the Halo Photonics lidar in the field. The virtual lidar is configured in staring mode, aimed upstream up to $7D$ from the turbine. Data are collected with 2-m spatial resolution and a 1-Hz sampling frequency for 10 minutes after the wind turbine wake is developed. Then, lidar range weighting according to Eq. 4 is applied to generate a lidar-equivalent wind speed signal. The virtual lidar signal is used to assess the impact of volume averaging on the fitting parameters, indicating that lidar underestimates σ due to the attenuation of the energy of the signal, and overestimates the length-scale due to the smoothing of the fluctuations. A quantitative analysis of the impact of range-gate sizes on these parameters for the particular numerical simulation corresponding to a neutral boundary layer is shown in Figure 5. From the current results, it is projected that the impact of volume averaging is significant during stable atmospheric boundary conditions, and the predictions of the fitting parameters which are dependent on σ and L will exhibit more bias. An explanation of this comment can be achieved by checking the length-scale obtained for the different cases. Case01 has a TI of 1.24% and the calculated length-scale, L, is

477 m, while Case03 has a TI of 3.5% and length-scale, L, of 142 m. The smoothing of turbulent fluctuations caused volume averaging is more pronounced for Case01 than Case03.
An attempt has been made to use the lidar data to predict the coherence based on the field campaign data. Two approaches are taken to predict coherence based on the lidar measurements: approach 1) least-squares fitting of the lidar measured coherence and coherence model up to a wavenumber corresponding to $\gamma^2 \geq 0.5$ (Figure 4b, e, h) and approach 2) minimizing the error between lidar-measured coherence and the coherence model with volume averaging included (Figure 4c, f, i). Both approaches perform well in terms of retrieving the coherence, whereas the second approach is computationally costlier than the first approach. A comparative quantification of the fitting parameters is provided in Table 1 for Simley's theoretical coherence model and the derived coherence from lidar measurements. Fitting parameters for the derived coherence are far different than the Simley's model, except for Case02 where the bias in the σ and L estimates is expected to be low.

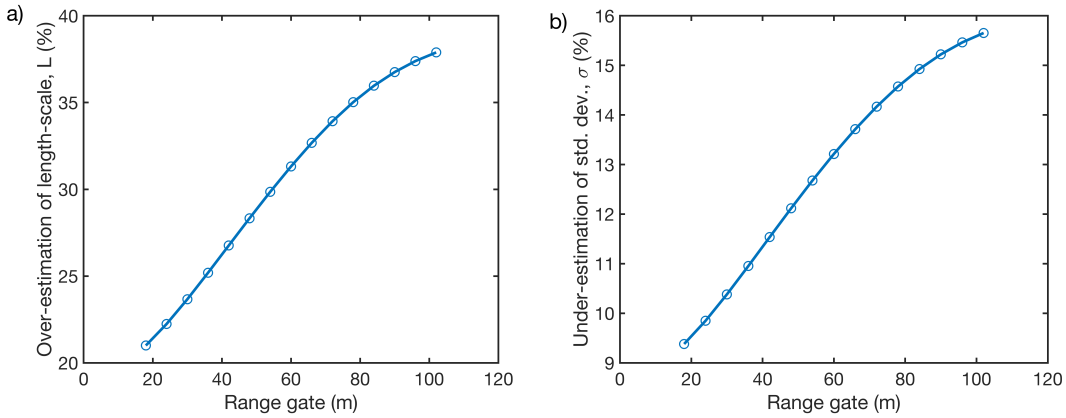

Figure 5: Impact of volume averaging on the theoretical coherence parameters. a) length-scale; b) standard deviation.

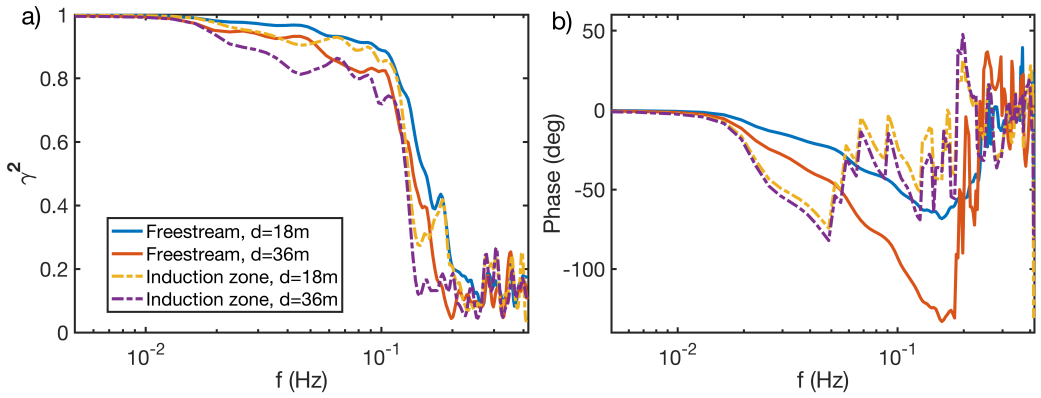

Figure 6: Impact of induction zone on lidar-measured coherence. a) Coherence; b) phase angle.

5. Impact of induction zone

Lidar data are separated into freestream and induction zone regions based on the mean wind speed profiles shown in Figure 1a. Freestream is defined as further upstream of two rotor

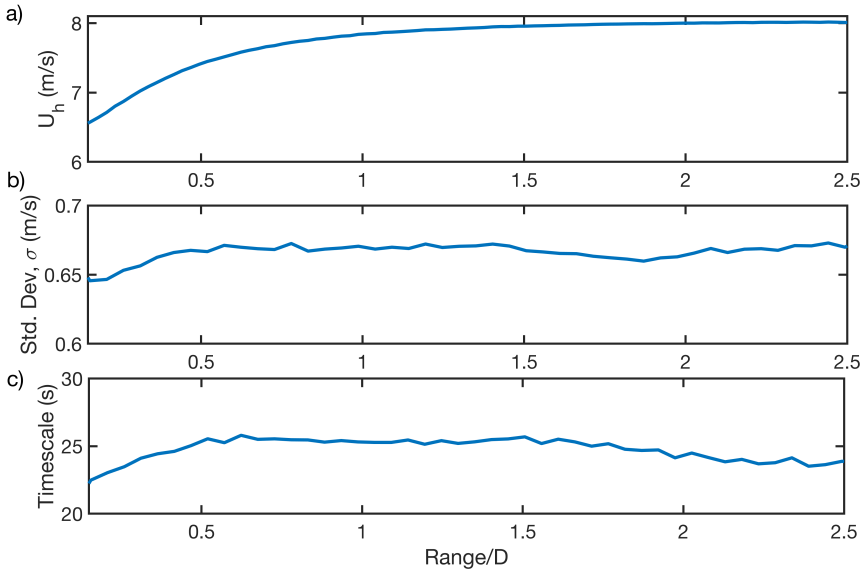

Figure 7: Large-eddy simulation and virtual lidar data. a) 10-min averaged wind speeds for different upstream distances from the turbine; b) standard deviation, σ, of the 10-min wind speed measurements; c) integral time-scale, T_{xx}, of the data for different upstream distances from the turbine.

diameters from the turbine, and induction zone is defined within two rotor diameters from the turbine. Coherence and phase-angle calculations based on the freestream data and induction zone data show that there are no significant effects of the induction zone on the coherence (Figure 6). However, there are differences in the phase angle. In particular, the maximum coherent wavenumber within the induction zone is lower than the freestream region, which suggests that prediction of turbulent structures in the induction zone is not the same as in the freestream region. The coherence and phase angle for Case03 is shown in Figure 6. Note that nearest lidar measurement point is 82 m upstream of the turbine where turbine diameter, D, is 77 m. Therefore, investigation within the dominant induction zone which is close to the turbine is restricted.

To further investigate the impact of the turbine induction zone on the coherence model and turbulent structures, virtual lidar data collected through the numerical simulation are used. Data are time averaged to see the reduction of wind speed in front of the turbine (Figure 7a). A substantial reduction in wind speed of 16.25% is observed. As the magnitude of the mean wind speed has dropped in the induction zone, it is expected that the standard deviation of the wind speed will also drop. However, a significant drop is not observed (see Figure 7b). As lidar data show that the phase angle in the induction zone is different, the time-scale of the virtual lidar is also calculated. It is seen that time-scale drops close to the turbine. The drop is prominent closer to the turbine where the wind speed drop is significant. Therefore, the length-scale, L, (Eq. 2) which is calculated based on the time-scale and mean wind speed will be different in this region. If the freestream theoretical coherence model is applied close to the turbine based on the parameters calculated in the induction zone, the length-scale parameter needs to be adjusted.

6. Conclusions

While the coherence in the induction zone is not substantially different than in the freestream, the phase of the turbulent structures is easily differentiated. The time-scale drops as the wind approaches the turbine. However, the overall fluctuation of the wind speed does not change substantially because of the slowdown of the wind speed in front of the turbine. Volume averaging creates a bias in the coherence measurements – it overpredicts coherence in the low wavenumber and underpredicts in high wavenumber. Furthermore, to allow practical applications of the lidar data, an analytical formulation of lidar-measured longitudinal coherence, dependent on the lidar

properties has been developed. The corrected coherence can be predicted based on wind speed data collected with a lidar. Different cases used in this study suggest that coherence is highly dependent on the atmospheric stability, and Simley's approach to consider the atmospheric stability through length-scale and standard deviation is a good approach. However, lidar data overestimate length-scale and underestimate standard deviation. A longer field campaign is needed to develop a lidar data-driven generic longitudinal coherence model.

7. Acknowledgments

This work was authored [in part] by the National Renewable Energy Laboratory, operated by Alliance for Sustainable Energy, LLC, for the U.S. Department of Energy (DOE) under Contract No. DE-AC36- 08GO28308. Funding provided by the U.S. Department of Energy Office of Energy Efficiency and Renewable Energy Wind Energy Technologies Office. The views expressed in the article do not necessarily represent the views of the DOE or the U.S. Government. The U.S. Government retains and the publisher, by accepting the article for publication, acknowledges that the U.S. Government retains a nonexclusive, paid-up, irrevocable, worldwide license to publish or reproduce the published form of this work, or allow others to do so, for U.S. Government purposes. Matthew Churchfield is acknowledged for implementing the virtual lidar function in the Simulator fOr Wind Farm Applications (SOWFA) code.

References

[1] A. Scholbrock, P. Fleming, D. Schlipf, A. Wright, K. Johnson, and N. Wang. Lidar-enhanced wind turbine control: Past, present, and future. In *2016 American Control Conference (ACC)*, pages 1399–1406, July 2016.

[2] J. Mann, A. Peña, N. Troldborg, and S. J. Andersen. How does turbulence change approaching a rotor? *Wind Energy Science*, 3(1):293–300, 2018.

[3] G. I. Taylor. The spectrum of turbulence. *Proceedings of the Royal Society of London. Series A*, 164(919):476–490, 1938.

[4] A. G. Davenport. The spectrum of horizontal gustiness near the ground in high winds. *Quarterly Journal of the Royal Meteorological Society*, 87(372):194–211, 1961.

[5] E. Simley and L. Y. Pao. A longitudinal spatial coherence model for wind evolution based on large-eddy simulation. In *2015 American Control Conference (ACC)*, pages 3708–3714, July 2015.

[6] S. Davoust and D. von Terzi. Analysis of wind coherence in the longitudinal direction using turbine mounted lidar. *Journal of Physics: Conference Series*, 753:072005, sep 2016.

[7] D. Schlipf, F. Haizmann, N. Cosack, T. Siebers, and P. Cheng. Detection of wind evolution and lidar trajectory optimization for lidar-assisted wind turbine control. *Meteorol. Zeitschrift*, 24(6):565–579, 11 2015.

[8] E. Simley, L. Y Pao, P. Gebraad, and M. Churchfield. Investigation of the impact of the upstream induction zone on LIDAR measurement accuracy for wind turbine control applications using large-eddy simulation. *Journal of Physics: Conference Series*, 524:012003, 2014.

[9] Matthew J. Churchfield, Sang Lee, John Michalakes, and Patrick J. Moriarty. A numerical study of the effects of atmospheric and wake turbulence on wind turbine dynamics. *Journal of Turbulence*, 13:N14, 2012.

[10] J. K. Lundquist, M. J. Churchfield, S. Lee, and A. Clifton. Quantifying error of lidar and sodar doppler beam swinging measurements of wind turbine wakes using computational fluid dynamics. *Atmospheric Measurement Techniques*, 8(2):907–920, 2015.

[11] A. R. Meyer Forsting, N. Troldborg, and A. Borraccino. Modelling lidar volume-averaging and its significance to wind turbine wake measurements. *Journal of Physics: Conference Series*, 854(1), 2017.

[12] R. Frehlich, Y. Meillier, M. Jensen, B. Balsley, and M. Sharman. Measurements of boundary layer profiles in an urban environment. *Applied Meteorology and Climatology*, 46(6):821–837, 2006.

[13] R. Thresher, W. Holley, C Smith, N Jafarey, and S.-R. Lin. Modeling the response of wind turbines to atmospheric turbulence. Technical report, Department of Mechanical Engineering, Oregon State University, 1981.

[14] E. Simley. *Wind Speed Preview Measurement and Estimation for Feedforward Control of Wind Turbines*. PhD thesis, Boulder, CO, USA, 2015.

[15] L. Kristensen. On longitudinal spectral coherence. *Boundary-Layer Meteorology*, 16:145–153, jun 1979.